

Free-Form Micro-Optics Enabling Ultra-Broadband Low-Loss Off-Chip Coupling

Shaoliang Yu, Luigi Ranno, Qingyang Du, Samuel Serna,* Colin McDonough, Nicholas Fahrenkopf, Tian Gu,* and Juejun Hu

Efficient fiber-to-chip coupling has been a major hurdle to cost-effective packaging and scalable interconnections of photonic integrated circuits. Conventional photonic packaging methods relying on edge or grating coupling are constrained by high insertion losses, limited bandwidth density, narrow band operation, and sensitivity to misalignment. This work presents a new fiber-to-chip coupling scheme based on free-form reflective micro-optics. A design approach which simplifies the high-dimensional free-form optimization problem to as few as two full-wave simulations is implemented to empower computationally efficient design of high-performance free-form reflectors while capitalizing on the expanded geometric degrees of freedom. This work demonstrates fiber array coupling to waveguides taped out through a standard foundry shuttle run and backend integrated with 3-D printed micro-optics. A low coupling loss down to 0.5 dB is experimentally measured at 1550 nm wavelength with a record 1-dB bandwidth of 300 nm spanning O to U bands. The coupling scheme further affords large alignment tolerance, high bandwidth density, and solder reflow compatibility, qualifying it as a promising optical packaging solution for applications such as wavelength division multiplexing communications, broadband spectroscopic sensing, and nonlinear optical signal processing.

1. Introduction

Photonic integrated circuits (PICs), the optical analog of electronic integrated circuits, are emerging as a mainstream technology in place of traditional bulky optical systems. Volume manufacturing leveraging standard semiconductor foundry processes have been driving steady cost down scaling and performance improvement of PICs, underpinning their widespread deployment in applications including communications, sensing, medical imaging, computing, quantum information, and navigation. Photonic packaging, an essential step to optically interface PICs with other components (in particular optical fibers) to form a functional system, is however increasingly becoming the bottleneck for PIC applications, since it often requires customized tools with low throughput and accounts for up to 80% of photonic module costs.^[1,2]

The “packaging bottleneck” results from the more stringent alignment tolerance, wavelength dependence, and sensitivity to optical losses inherent to optical coupling between different components, making it difficult to harness the existing electronic packaging infrastructure to significantly lower cost and boost throughput. To put this in context, Table S1 (Supporting Information) compares different fiber-to-chip coupling approaches, including edge and grating coupling which are commonplace in traditional photonic packaging as well as emerging coupling techniques.^[3,4] Edge coupling requires access to chip facets/edges, which not only precludes wafer-level testing but also limits bandwidth density due to the large 1-D fiber pitch. On the other hand, while diffractive grating coupling is compatible with wafer-level characterization, it is narrow-band and unsuitable for wavelength division multiplexing (WDM) or broadband sensing. **Figure 1** summarizes the insertion loss and 1-dB bandwidth performances of various fiber-to-chip coupling schemes demonstrated to date. Notably, while sub-1 dB coupling losses have been reported for both schemes, silicon photonic foundries typically specify coupling losses of 1.5 dB (edge) and 3 – 4 dB (grating),^[5,6] since special structures such as embedded metal mirrors or multilayer poly-Si overlay required for high-efficiency designs are not available in standard foundry runs.

In this paper, we report a universal photonic coupling scheme based on free-form micro-optical reflectors as illustrated in

S. Yu, L. Ranno, Q. Du, S. Serna, T. Gu, J. Hu
Department of Materials Science and Engineering
Massachusetts Institute of Technology
Cambridge, MA USA
E-mail: ssernaotalvaro@bridgew.edu; gutian@mit.edu

S. Serna
Department of Physics
Photonics and Optical Engineering
Bridgewater State University
Bridgewater, MA USA

C. McDonough, N. Fahrenkopf
The Research Foundation for State University of New York
State University of New York Polytechnic Institute
Albany, NY USA

T. Gu, J. Hu
Materials Research Laboratory
Massachusetts Institute of Technology
Cambridge, MA USA

 The ORCID identification number(s) for the author(s) of this article can be found under <https://doi.org/10.1002/lpor.202200025>

© 2023 The Authors. Laser & Photonics Reviews published by Wiley-VCH GmbH. This is an open access article under the terms of the Creative Commons Attribution-NonCommercial-NoDerivs License, which permits use and distribution in any medium, provided the original work is properly cited, the use is non-commercial and no modifications or adaptations are made.

DOI: 10.1002/lpor.202200025

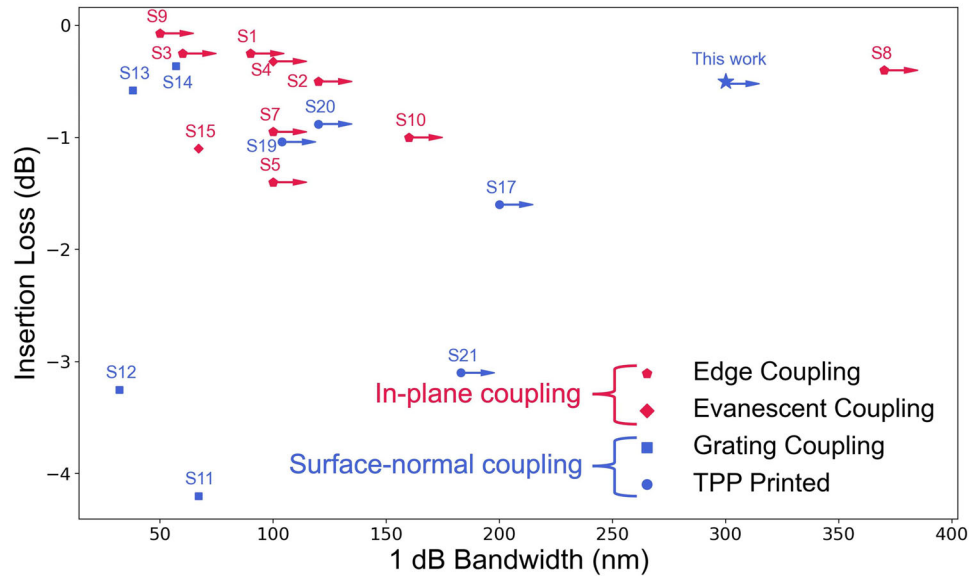


Figure 1. Summary of insertion loss and 1-dB bandwidth performances of fiber-to-chip coupling techniques demonstrated to date: the arrows indicate that the 1-dB bandwidth of the coupler exceeds the measurement wavelength range. Corresponding literature references and detailed quantitative information are tabulated in Section S1 (Supporting Information).

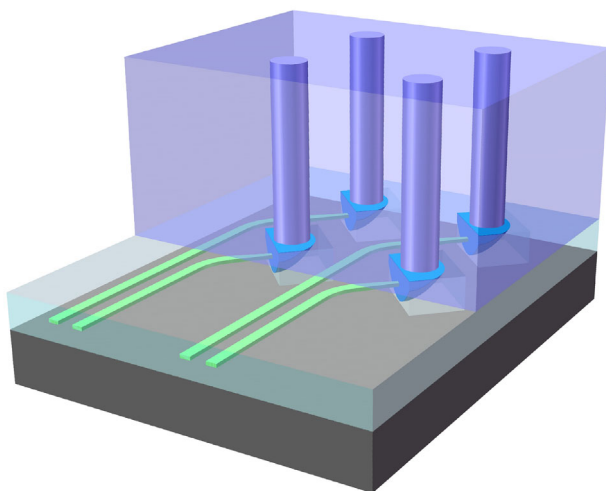


Figure 2. 3-D rendering of the free-form micro-optical fiber-to-chip coupling structure.

Figure 2. Unlike diffraction or refraction, optical reflection is inherently wavelength agnostic and incurs vanishingly low optical loss in the total internal reflection (TIR) regime. The reflectors serve to redirect and shape the waveguide output, enabling high-density surface-normal coupling to 2-D fiber arrays with low losses and high tolerance to misalignment. Fabrication of the micro-optical reflectors makes use of two photon polymerization (TPP), an additive 3-D printing technique offering subwavelength resolution ideal for free-form micro-optics definition.^[7–14] Original work from several groups has successfully implemented TPP for optical coupling between passive waveguides,^[15] lasers,^[16] free space,^[17] and fibers.^[18–24] Besides acting as an optical coupling element, TPP-written structures

have also been used as optomechanical supports to enhance alignment accuracy during photonic assembly.^[25,26] These pioneering results validate TPP as a viable technique for robust and versatile photonic packaging that is maturing into the commercial domain.^[27] Nonetheless, these early demonstrations still leave ample room for improvements on key aspects such as design, fabrication, and integration. The minimal fiber-to-chip coupling loss remains at ≈ 1 dB and above. Moreover, the aforementioned fiber-to-chip coupling designs operate exclusively with unclad waveguides and therefore entail custom top cladding striping steps, which are usually not part of standard photonic foundry processes. Last but not least, geometric fidelity of the TPP-written coupler structures has not been vetted upon heat treatment, which is necessary to establishing solder reflow compatibility of TPP-based packaging techniques.

The research reported herein is poised to circumvent these limitations. The couplers are designed for waveguides embedded inside dielectric claddings, the norm for foundry-processed PICs. We experimentally demonstrated a coupling loss of 0.5 dB, representing the lowest loss figure reported for surface-normal couplers at 1550 nm wavelength. The high efficiency benefits from the free-form reflector design, which allows full utility of the geometric degrees of freedom to precisely shape the wavefront and thereby facilitating fiber-to-waveguide mode matching. Our coupler further achieves ultrawide band operation with a record 1-dB bandwidth of 300 nm and coupling losses consistently below 2 dB across the entire second and third telecom windows (O, E, S, C, L, and U bands). Finally, we proved that the couplers' geometric fidelity and hence coupling efficiency are not compromised upon heat treatment up to 250 °C, the upper bound of typical nonlead solder reflow temperature. The combination of low loss, broadband operation, high bandwidth density, as well as wafer-scale testing and solder reflow compatibility qualify our approach as a promising optical interfacing solution for applications such as

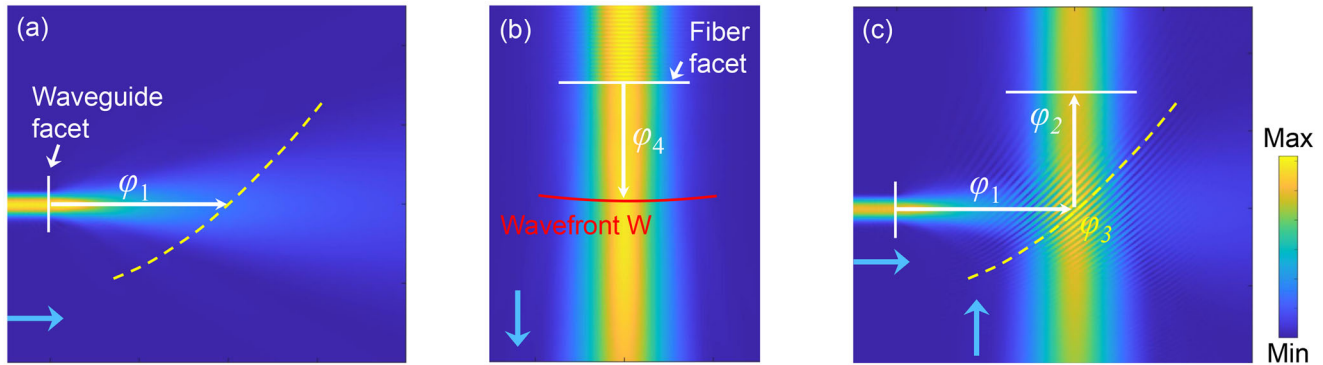


Figure 3. The free-form reflector design method based on wavefront interference. a,b) Finite-difference time-domain (FDTD) simulated field intensity profiles with separate optical outputs from a) the waveguide and b) the fiber, where the arrows denote phase delays. c) Concurrent modeling of the waveguide output and the back-propagated fiber output. Fringes due to interference between the two beams correspond to traces having a constant optical path linking the waveguide and the fiber (labeled with the dotted curve).

WDM communications, low coherence interferometry, quantum optics, on-chip optical tweezing, and spectroscopic sensing.

2. Wavefront-Based Free-Form Micro-Optical Coupler Design

Free-form optics, which are characterized by surfaces with no axis of rotational invariance,^[28] confer on-demand wavefront control taking advantage of the large number of accessible degrees of freedom. The geometric flexibility, however, poses a design challenge if the full design space is to be explored. Design of free-form optics largely relies upon parameterization of the surface geometry (e.g., polynomial expansion) and subsequent multidimensional optimization. The computation overhead for solving such optimization problems in the 3-D full-vectorial regime is often rather cumbersome.

Here we propose a design approach based on wavefront interference which simplifies the free-form design problem into minimally two finite-difference time-domain (FDTD) simulations. The approach is illustrated in **Figure 3**, where our task is to search for a reflective surface geometry that transforms the in-plane waveguide mode to the out-of-plane fiber mode in an orthogonal direction, or performs other mode matching functions. The Fermat's principle specifies that the total optical path length connecting the two modes' wavefronts while passing through the reflector must be stationary with respect to variations of the path, i.e.

$$\varphi_1 + \varphi_2 + \varphi_3 = \varphi_{\text{tot}} \quad (1)$$

where φ_1 and φ_2 correspond to the phase delays associated with light traveling from the waveguide to the reflector and from the reflector to the fiber, respectively, φ_3 is the phase delay incurred by TIR at the reflector, and φ_{tot} is a constant. As we show in the Section S2 (Supporting Information), φ_3 is only weakly dependent on the light incidence location on the reflector and thus can be treated as a constant and will henceforth be absorbed into φ_{tot} .

Next, we consider the configuration in **Figure 3b** which models light output from the fiber in the absence of the waveguide and the reflector. In the figure, the red curve (marked as W) labels

the wavefront of light exiting from the fiber after propagating for some distance in free space. We denote the phase delay from fiber to W as φ_4 , which is a constant independent of the light path. Now if we back propagate the light from W to the fiber, the phase delay from W to a point on the reflector is given by $\varphi_4 - \varphi_2$. Equation (1) translates to:

$$\varphi_1 - (\varphi_4 - \varphi_2) = \varphi_{\text{tot}} - \varphi_4 \equiv 2N\pi \quad (2)$$

Here $\varphi_{\text{tot}} - \varphi_4$ is a constant and we set it to integral multiples of 2π . This is possible since we can always tune the position of W such that N becomes an integer. Equation (2) implies that when output from the waveguide and the back propagated fiber mode from W co-propagate in space, the loci of constructive interference (given by Equation 2) coincide with a group of reflector surface shapes that satisfy the Fermat's principle. The optimal reflector geometry is then uniquely determined by choosing a surface from the group which maximizes overlap integral between the waveguide output and the back propagated fiber mode over the surface.

The design approach outlined here is deterministic and requires only two 3-D FDTD simulations: the fiber mode propagation without the waveguide, and co-propagation of the waveguide output and the back propagated fiber mode. Once the second simulation is complete, we extract the loci of maximum local intensity points using a spiral trace search algorithm (Section S3, Supporting Information). The electromagnetic field components on the surface coordinates are subsequently used to evaluate the overlap integral. In addition to providing a computationally efficient route for optimization of waveguide coupling to standard single-mode fibers, we further show that the method is also applicable to designing unconventional coupler structures. As an example highlighting versatility of the approach, we designed a micro-optical coupler between a SiN waveguides and a polarization-maintaining endlessly single-mode photonic crystal fiber, with the latter having an irregular mode profile without circular symmetry (Section S4, Supporting Information). The design claims a peak coupling efficiency of 91.8% (0.37 dB insertion loss) and a 1-dB bandwidth exceeding 500 nm. Such a design potentially enables efficient coupling of broadband light (e.g., supercontinuum) between on-chip waveguides and fibers

while maintaining single-mode operation with octave-spanning bandwidth.

3. Device Fabrication and Characterization

As a proof of concept, here we demonstrate integration of the free-form couplers with foundry-processed SiN waveguides, while the reflective coupler configuration is equally applicable to silicon-on-insulator waveguides with similar low-loss, ultra-broadband performance (Section S5, Supporting Information). The SiN waveguides were fabricated on an American Institute for Manufacturing Integrated Photonics (AIM Photonics) multi-project wafer (MPW) shuttle run.^[29] Figure 4a schematically depicts the cross-sectional structure of the fabricated device. The SiN waveguides, designed to support a single TE-polarization mode, are 1500 nm in width and are adiabatically tapered to a width of 360 nm at the end tips. The length of the inverse tapers is set to be 100 μm to eliminate the mode conversion loss (Section S6, Supporting Information) and filter high order components, hence ensuring single-mode operation throughout the spectral range of interest. The recesses, which have a depth of 140 μm and act to expose the waveguide's vertical facets for coupler attachment, are defined during the dicing trench patterning step via reactive ion etching as part of the standard shuttle run process flow. The micro-optical couplers were subsequently fabricated using TPP, and details of the fabrication process are elaborated in Experimental Section. The writing time of the coupler structure is 193 s. The fact that the coupler comprises only a single block with a small surface-to-volume ratio allows the writing time to be vastly reduced to 12 s by resorting to a shell-and-scaffold^[30] printing mode, where only the shell of the structures is written by TPP, followed by removing excess resin and then UV flood exposure to polymerize the core of the structure enclosed by the shell (Section S7, Supporting Information). Avoiding long polymer waveguide couplers that preclude efficient shell-and-scaffold printing is another advantage of our coupler architecture. Figure 4b presents a top-view optical micrograph of the finished chip and Figure 4c furnishes a close-up view of the coupler structure. The couplers exhibit excellent adhesion to the waveguide facets with no sign of mechanical failure. The coupler surfaces feature a low root-mean-square roughness of 18 nm, implying negligible optical losses due to roughness scattering.

Figure 5 summarizes FDTD modeling results on the fabricated coupler structure, which is optimized to couple TE-polarized light from a SiN waveguide to an SMF-28 fiber. Leveraging the capability of free-form reflective surfaces in precise wavefront shaping, the intensity profile of the beam exiting from the coupler closely matches that of the fiber mode (Figure 5a), which accounts for the exceptionally low coupling loss: <1 dB throughout the second and third telecom windows (1260–1675 nm, Figure 5c). The in-plane transitional alignment tolerance corresponding to 1-dB loss penalty is $\pm 2.2 \mu\text{m}$, consistent with the fiber mode field diameter (Figure 5d). The 1-dB angular alignment tolerance is simulated to be 2° for both roll and pitch tilt of fiber (Section S8, Supporting Information). In the out-of-plane direction, the reflected beam is almost collimated, giving rise to negligible (< 0.1 dB) loss penalty over a distance range of 28 μm (Figure 5e). The translational alignment tolerance can be further

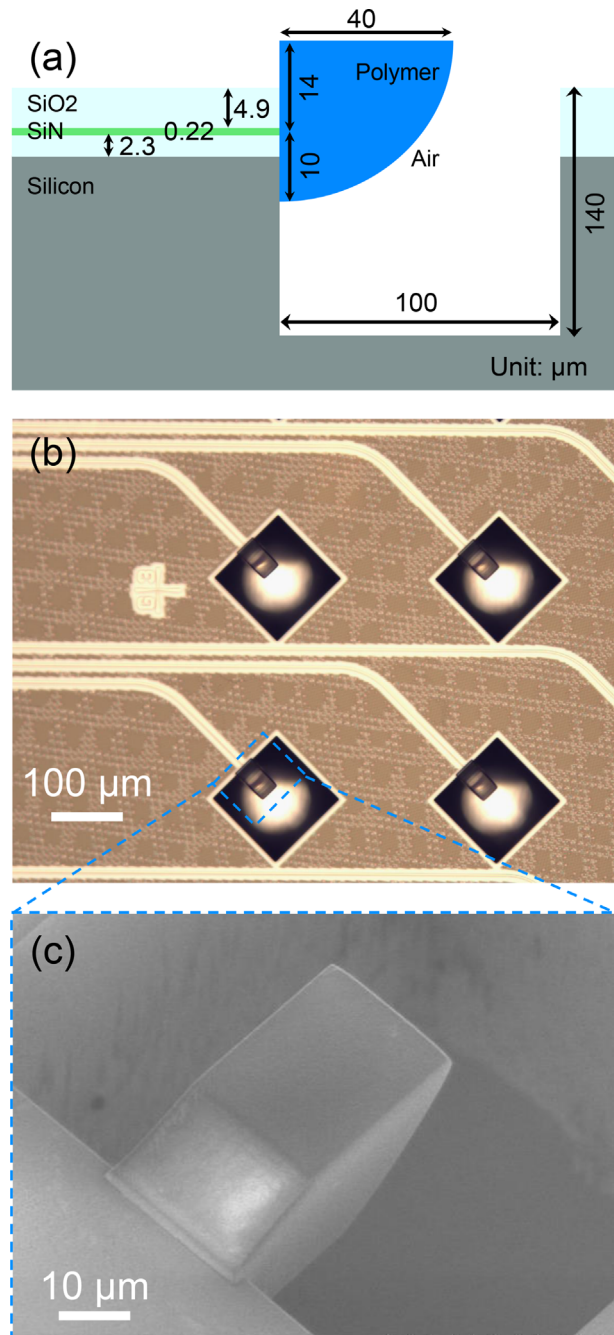


Figure 4. a) Schematic cross-section of the microreflector (not drawn to scale). The dimensions (in μm) are marked. b) Top-view optical micrograph of the foundry-processed chip. c) Close-up view of the coupler structure.

enhanced by expanding the output beam diameter and writing an additional lensing structure on the fiber facet.

We also studied the fabrication tolerance of the coupler with respect to misalignment during TPP writing as well as non-vertical waveguide facet profiles. The excess insertion loss induced by misalignment between the free-form reflector and the waveguide during TPP fabrication is quantified in Section S9

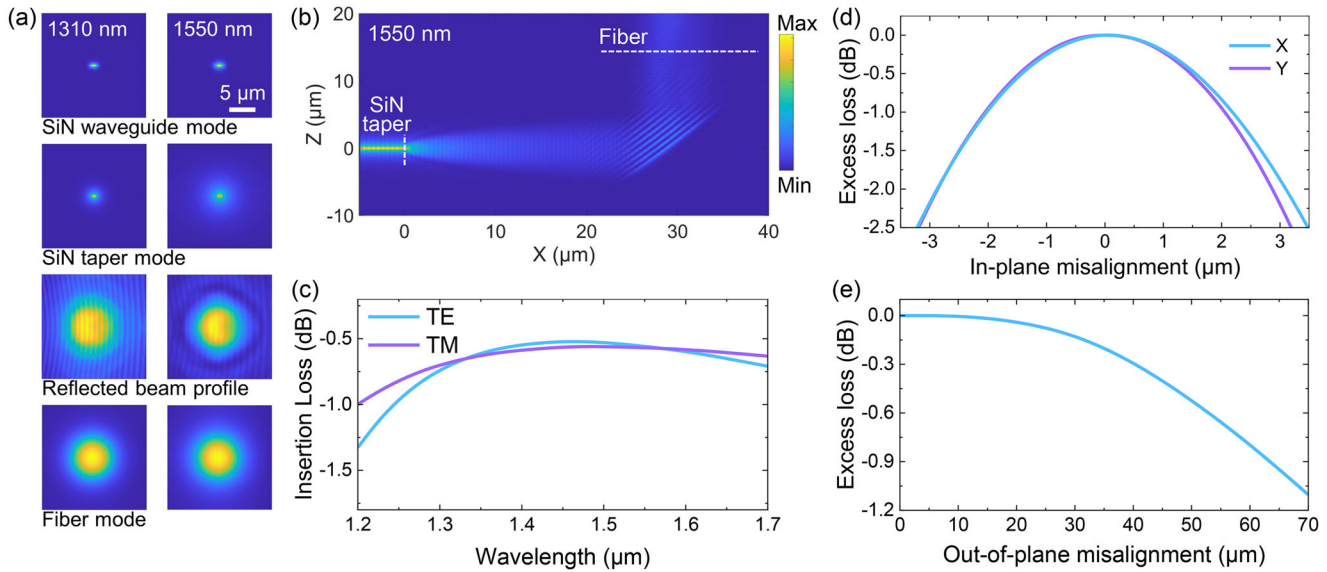


Figure 5. The micro-optical coupler modeled using 3-D finite-difference time-domain (FDTD). a) The mode profiles of the SiN waveguide and SiN taper, the reflected beam from the freeform coupler and the fundamental mode of single mode fiber at 1310 and 1550 nm, respectively. b) Simulated electric field intensity distribution across the waveguide center plane. c) Modeled insertion loss spectrum; and d,e) alignment tolerances along d) in-plane and e) out-of-plane directions.

(Supporting Information), showing a simulated 1-dB translational tolerance of $1.8 \mu\text{m}$, which can be partially compensated by shifting the fiber position (Figure S8a, Supporting Information). Given our experimentally demonstrated alignment accuracy of $<0.16 \mu\text{m}$,^[24] the excess loss is negligible. Since the refractive index of the coupler is approximate to the effective index of the SiN taper mode, the performance of the coupler is largely immune to the nonvertical sidewall angle of the deep trench (Figure S8b, Supporting Information).

Optical waveguides with micro-optical couplers attached to both of their input and output facets were tested using SMF-28 fiber arrays with an inter-fiber pitch of $250 \mu\text{m}$, matching that of the couplers on-chip (Figure 6a). Wavelength-dependent coupling losses were inferred from the total insertion loss of the coupler-waveguide-coupler loop, after subtracting propagation loss contributions from the waveguide. Detailed experimental characterization protocols are discussed in the Experimental Section. Figure 6b plots the measured loss spectra of the coupler. At 1550 nm wavelength, the coupler boasts a low coupling loss of 0.5 dB consistent with our modeling result. The 1-dB bandwidth covers over 300 nm from 1340 to 1640 nm, whose upper bound is only limited by the accessible wavelength range of our lasers. Over the measured wavelength range from 1260 to 1640 nm, the coupling loss is below 2 dB, enabling the coupler to be used for WDM applications spanning the entire long-wave telecom bands. In fact, we have experimentally observed coupling of visible light from a fiber into and out of the chip through the couplers as well (Figure 6c), although the coupling efficiency was not quantified given the multimode nature of the SiN waveguides at wavelengths below 1260 nm. The slight deviation from the simulation result is attributed to shape distortion of the reflector likely caused by polymer volume shrinkage during crosslinking, as well as overtone absorption of the polymer which accounts for the loss peak at 1380 nm wavelength (Section S10, Supporting

Information). Due to mode leakage to the silicon substrate, the experimental result shown considerable wavelength-dependent loss for the TM mode, which can be mitigated with a thicker undercladding layer (Section S11, Supporting Information). We also verified that the coupling loss remained unchanged after heat treatment at $250 \text{ }^\circ\text{C}$ (Figure 6d), a key proof validating solder reflow compatibility of the micro-optical coupler technology. The in-plane 1-dB alignment tolerance is $\pm 2.2 \mu\text{m}$ (Figure 6e), commensurate with the positioning accuracy of high-precision passive alignment instruments. In accordance with the simulation result in Figure 5, the coupler is insensitive to longitudinal offset between the fiber and the coupler with an out-of-plane 1-dB alignment tolerance of $20 \mu\text{m}$.

4. Discussion

The low-loss and broadband micro-optical coupler technology provides a promising optical coupling platform for integrated photonics packaging in applications spanning WDM communications,^[31] spectroscopic sensing,^[32] nonlinear frequency generation,^[33] biomedical imaging,^[34] and optical computing.^[35] As an example showcasing the potential application of the technology in nonlinear optics, we contrasted the nonlinear characteristics of SiN waveguides terminated with the free-form micro-optical couplers and standard grating couplers (but are otherwise identical). In Figure 7a, transmission spectra of the waveguides were obtained with femtosecond pulse trains with a repetition rate of 100 MHz, an average power of 80 mW, and a pulse duration of 100 fs (corresponding to a peak power of 8 kW). When the pulses were launched through the grating couplers, the resulting spectrum (purple curve) is truncated due to limited bandwidth of the grating couplers. In contrast, the micro-optical coupler preserved spectral information of the pulses (blue curve). Figure 7b compares spectral broadening

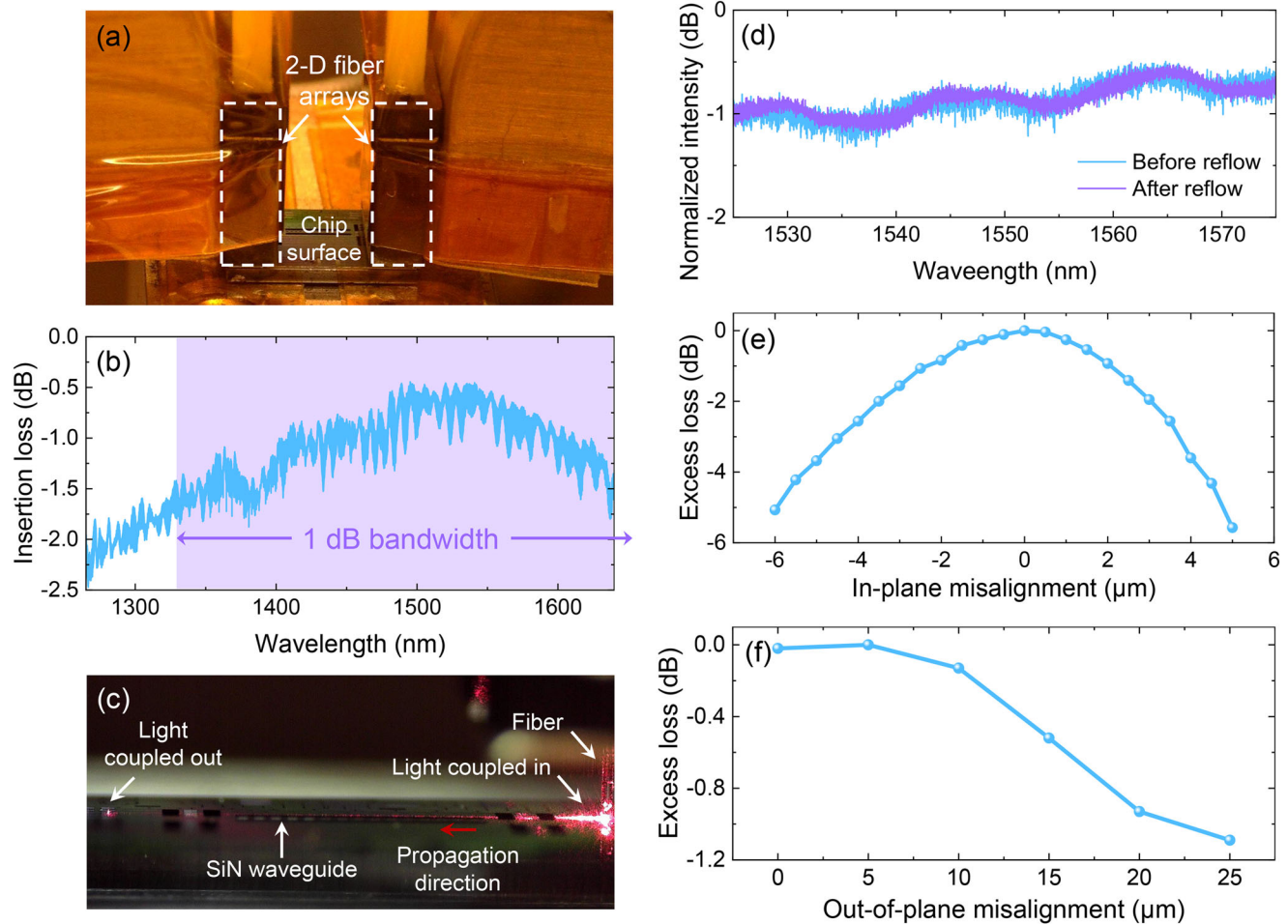


Figure 6. a) A photo of 2-D fiber arrays coupling to on-chip waveguides via the reflective couplers. b) Measured broadband insertion loss of the coupler. c) A photo showing visible light coupling into and out of a waveguide via the same coupler designed for 1550 nm wavelength. d) Transmission spectra before (blue) and after (purple) annealing at 250 °C to simulate solder reflow heat treatment. e, f) Measured e) in-plane and f) out-of-plane alignment tolerances.

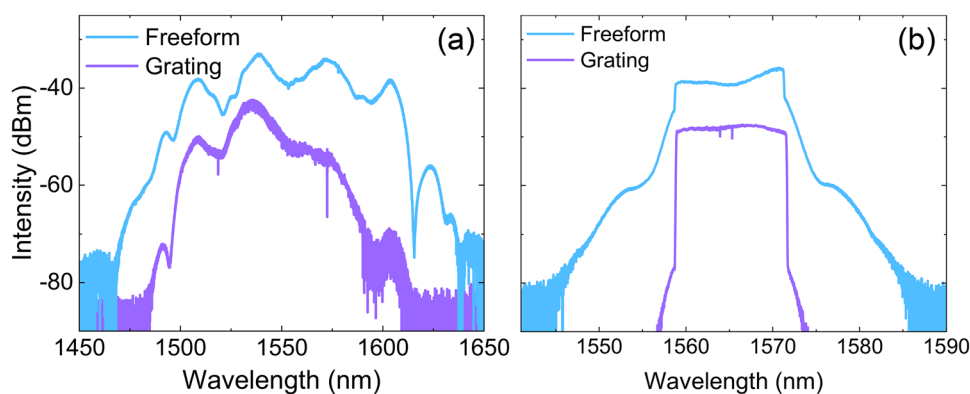


Figure 7. Transmission spectra of a) 100 fs femtosecond pulses with 8 kW peak power; and b) 13 nm wide top-hat pulses after spectral broadening due to self-phase modulation in SiN waveguides. The pulses were coupled into the waveguides via the free-form micro-optical couplers (blue curves) and grating couplers (purple curves) with identical input power.

due to self-phase modulation in SiN waveguides upon injection of 13 nm wide top-hat pulses centered around 1565 nm wavelength, showing that the nonlinear broadening is far more pronounced in waveguides with the micro-optical couplers. This enhanced nonlinearity benefits from the high coupling efficiency and hence higher on-chip optical power, as well as the micro-optical coupler's wide bandwidth which minimizes spectral distortion. Importantly, no sign of optical damage was observed in the micro-optical couplers after pumping using ultrafast pulses with peak powers up to 8 kW. The unique combination of low loss, large bandwidth and high power stability qualifies the micro-optical couplers as a robust optical interface of choice for nonlinear photonic device packaging and characterization, where broadband and highly efficient coupling interfaces are of paramount importance, e.g., for nonlinear frequency generation.^[36]

Besides functioning as a fiber-to-chip coupling interface, the micro-optical free-form reflectors can also be applied to enable efficient chip-to-chip and chip-to-interposer coupling. Solder-reflow compatibility of the couplers implies that they can be implemented alongside solder bonds to form flip-chip optical and electrical connections between two chips concurrently with potential self-alignment capability, owing to the large misalignment tolerance of the couplers. An instance of the simultaneous optical and electrical connection design is illustrated in Section S12 (Supporting Information). The free-form reflector further offers a versatile method to control the wavefront and beam shape of light coupling from on-chip waveguides to free space, a feature instrumental to applications such as free space communications, remote sensing, optical manipulation,^[17] and quantum optics.^[37]

In summary, we demonstrated a fiber-to-chip coupling scheme leveraging micro-optical reflectors which are integrated on standard foundry-processed photonic chips. The free-form couplers are designed using a wavefront-based, computationally efficient approach which avoids time-consuming parameter search used in traditional free-form optics design. Experimentally fabricated couplers measure a low insertion loss of 0.5 dB at 1550 nm wavelength, a 1-dB bandwidth of >300 nm, and <2 dB coupling loss across the O to U telecom bands. Moreover, we have validated that the couplers are solder reflow compatible and can withstand high power pulses with peak power exceeding 8 kW. The same reflective coupler architecture is further applicable to efficient broadband chip-to-chip, chip-to-interposer, and chip-to-free-space coupling. We therefore anticipate that the universal micro-optical coupling interface will find widespread use spanning data communications, spectroscopic sensing, quantum optics, and nonlinear optical signal processing, among many other applications.

5. Experimental Section

Device Fabrication: The photonic chips were fabricated in a multiproject AIM shuttle run. The trenches used to expose the waveguide facets were defined during the dicing-trench etching step. Subsequently, microreflectors made of IP-n162 were printed on the side wall of the pre-defined trenches via TPP using a commercially-available machine (Photonic Professional GT, Nanoscribe GmbH) with the following printing parameters: hatching distance 100 nm, slicing distance of 200 nm, writing speed of 5 mm s⁻¹, and average writing power 60 mW (780 nm, 80 MHz, ≈100 fs).

Optical Characterization: The optical performance of the couplers was characterized using a tunable laser with built-in vector analyzer (OVA

5000). The broadband measurements were performed using three different tunable lasers from Santec's TSL series, controlled through an optical switch module (OSU-100). The nonlinear measurements were performed using the ELMO High Power-FS laser from Menlo Systems, which was coupled into a standard SMF-28 fiber through a free-space fiber coupler. Coupling was performed using SMF-28 fibers and fiber arrays cleaved at 0°. The chips were tested on an automated probe station (SD-100 from Maple Leaf Photonics). For the measurement of the insertion loss, the power transmitted through the device and received at the fiber output was first measured. A second measurement whereby the transmission through the chip is substituted by propagation along an SMF-28 fiber with length of ≈0.5 m (which adds negligible propagation loss) to account for the losses in the fiber connectors, and polarization controllers. The difference between the two measurements (after also taking into account the propagation loss through the SiN waveguide, which had been measured by a cutoff method) was used to determine the insertion loss of the combined input and output couplers. The loss of an individual coupler was then given as half of the combined input-output couplers loss.

Device Modeling: Optical simulations were performed using Ansys' Lumerical FDTD module. Optimization of the reflector surface was done using a home-written Python script. The extracted point cloud corresponding to the loci of constructive interference was output as 3-D STL file using Solidworks for FDTD simulation and TPP writing.

Supporting Information

Supporting Information is available from the Wiley Online Library or from the author.

Acknowledgements

This work was supported by ARPA-E under the ENLITENED Program (Award Number: DE-AR0000847). The authors thank Dr. Xiaoming Qiu and Anthony Zhou for their help with the modeling code development.

Conflict of Interest

The authors declare no conflict of interest.

Author Contributions

S.Y. and L.R. contributed equally to this work. S.Y., T.G., and J.H. conceived the device design. S.Y. and L.R. designed, fabricated, and characterized the devices. Q.D. assisted with device fabrication. S.S. and L.R. carried out the wide band and nonlinear measurements. C.M. and N.F. performed the foundry fabrication and helped with device design. S.Y., L.R., and J.H. drafted the manuscript. T.G. and J.H. supervised and coordinated the research. All authors contributed to revising the manuscript and technical discussions.

Data Availability Statement

The data that support the findings of this study are available from the corresponding author upon reasonable request.

Keywords

fiber-to-chip coupling, free-form optics, integrated photonics, two photon polymerization, photonic packaging

Received: January 14, 2022

Revised: October 17, 2022

Published online: March 12, 2023

- [1] T. Barwicz, T. W. Lichoulas, Y. Taira, Y. Martin, S. Takenobu, A. Janta-Polczynski, H. Numata, E. L. Kimbrell, J. W. Nah, B. Peng, D. Childers, R. Leidy, M. Khater, S. Kamlapurkar, E. Cyr, S. Engelmann, P. Fortier, N. Boyer, *Opt. Fiber Technol.* **2018**, *44*, 24.
- [2] L. Carroll, J.-S. Lee, C. Scarcella, K. Gradkowski, M. Duperron, H. Lu, Y. Zhao, C. Eason, P. Morrissey, M. Rensing, S. Collins, H. Hwang, P. O'Brien, *Appl. Sci.* **2016**, *6*, 426.
- [3] G. Son, S. Han, J. Park, K. Kwon, K. Yu, *Nanophotonics* **2018**, *7*, 1845.
- [4] R. Marchetti, C. Lacava, L. Carroll, K. Gradkowski, P. Minzioni, *Photonics Res.* **2019**, *7*, 201.
- [5] AIM Photonics, <https://www.aimphotonics.com/process-design-kit>
- [6] Advanced Micro Foundry, <https://www.advmf.com/wp-content/uploads/2019/08/AMF-Brochure-Web.pdf>
- [7] T. Gissibl, S. Thiele, A. Herkommer, H. Giessen, *Nat. Photonics* **2016**, *10*, 554.
- [8] M. Farsari, B. N. Chichkov, *Nat. Photonics* **2009**, *3*, 450.
- [9] J. Li, P. Fejes, D. Lorensen, B. C. Quirk, P. B. Noble, R. W. Kirk, A. Orth, F. M. Wood, B. C. Gibson, D. D. Sampson, R. A. McLaughlin, *Sci. Rep.* **2018**, *8*, 14789.
- [10] W. Xiong, Y. S. Zhou, X. N. He, Y. Gao, M. Mahjour-Samani, L. Jiang, T. Baldacchini, Y. F. Lu, *Light: Sci. Appl.* **2012**, *1*, e6.
- [11] C. Xiong, C. Liao, Z. Li, K. Yang, M. Zhu, Y. Zhao, Y. Wang, *Front. Mater.* **2020**, *7*, 586496.
- [12] H. Gao, G. F. R. Chen, P. Xing, J. W. Choi, H. Y. Low, D. T. H. Tan, *Adv. Opt. Mater.* **2021**, *9*, 1803.
- [13] T. Gissibl, S. Thiele, A. Herkommer, H. Giessen, *Nat. Commun.* **2016**, *7*, 11763.
- [14] D. Wu, S. Z. Wu, L. G. Niu, Q. D. Chen, R. Wang, J. F. Song, H. H. Fang, H. B. Sun, *Appl. Phys. Lett.* **2010**, *97*, 031109.
- [15] N. Lindenmann, G. Balthasar, D. Hillerkuss, R. Schmogrow, M. Jordan, J. Leuthold, W. Freude, C. Koos, *Opt. Express* **2012**, *20*, 17667.
- [16] M. R. Billah, M. Blaicher, T. Hoose, P.-I. Dietrich, P. Marin-Palomo, N. Lindenmann, A. Nesic, A. Hofmann, U. Troppenz, M. Moehrl, S. Randel, W. Freude, C. Koos, *Optica* **2018**, *5*, 876.
- [17] S. Yu, J. Lu, V. Ginis, S. Kheifets, S. W. D. Lim, M. Qiu, T. Gu, J. Hu, F. Capasso, *Optica* **2021**, *8*, 409.
- [18] P.-I. Dietrich, M. Blaicher, I. Reuter, M. Billah, T. Hoose, A. Hofmann, C. Caer, R. Dangel, B. Offrein, U. Troppenz, M. Moehrl, W. Freude, C. Koos, *Nat. Photonics* **2018**, *12*, 241.
- [19] N. Lindenmann, S. Dottermusch, M. L. Goedecke, T. Hoose, M. R. Billah, T. P. Onanuga, A. Hofmann, W. Freude, C. Koos, *J. Lightwave Technol.* **2015**, *33*, 755.
- [20] H. Luo, F. Xie, Y. Cao, S. Yu, L. Chen, X. Cai, *Opt. Lett.* **2020**, *45*, 1236.
- [21] H. Gehring, M. Blaicher, W. Hartmann, P. Varytis, K. Busch, M. Wegener, W. H. P. Pernice, *APL Photonics* **2019**, *4*, 010801.
- [22] H. Luo, L. Chen, S. Yu, X. Cai, *Opt. Lett.* **2021**, *46*, 4324.
- [23] H. Gehring, A. Eich, C. Schuck, W. H. P. Pernice, *Opt. Lett.* **2019**, *44*, 5089.
- [24] S. Yu, H. Zuo, X. Sun, J. Liu, T. Gu, J. Hu, *J. Lightwave Technol.* **2020**, *38*, 3358.
- [25] O. A. Jimenez Gordillo, S. Chaitanya, Y.-C. Chang, U. D. Dave, A. Mohanty, M. Lipson, *Opt. Express* **2019**, *27*, 20305.
- [26] P. S. Nair, J. Trisno, H. Wang, J. K. W. Yang, *Int. J. Extreme Manuf.* **2020**, *3*, 015301.
- [27] Technology - Vanguard Photonics, <https://www.vanguard-photonics.com/expertise/>.
- [28] J. Rolland, M. Davies, T. Suleski, C. Evans, A. Bauer, J. Lambropoulos, K. Falaggis, *Optica* **2021**, *8*, 161.
- [29] N. M. Fahrenkopf, C. McDonough, G. L. Leake, Z. Su, E. Timurdogan, D. D. Coolbaugh, *IEEE J. Sel. Top. Quantum Electron.* **2019**, *25*, 1.
- [30] A. S. Cordeiro, I. A. Tekko, M. H. Jomaa, L. Vora, E. McAlister, F. Volpe-Zanutto, M. Nethery, P. T. Baine, N. Mitchell, D. W. McNeill, R. F. Donnelly, *Pharm. Res.* **2020**, *37*, 174.
- [31] D. Zhang, D. Liu, X. Wu, D. Nesses, *J. Opt. Commun. Networking* **2020**, *12*, D99.
- [32] D. Kita, J. Michon, J. Hu, *Opt. Express* **2020**, *28*, 14963.
- [33] B. Shen, L. Chang, J. Liu, H. Wang, Q.-F. Yang, C. Xiang, R. N. Wang, J. He, T. Liu, W. Xie, J. Guo, D. Kinghorn, L. Wu, Q.-X. Ji, T. J. Kippenberg, K. Vahala, J. E. Bowers, *Nature* **2020**, *582*, 365.
- [34] X. Ji, D. Mojahed, Y. Okawachi, A. Gaeta, C. Hendon, M. Lipson, *Sci. Adv.* **2021**, *7*, eabg8869.
- [35] J. Feldmann, N. Youngblood, M. Karpov, H. Gehring, X. Li, M. Stappers, M. Gallo, X. Fu, A. Lukashchuk, S. Raja, J. Liu, C. Wright, A. Sebastian, T. Kippenberg, W. Pernice, H. Bhaskaran, *Nature* **2021**, *589*, 52.
- [36] B. Shen, L. Chang, J. Liu, H. Wang, Q. Yang, C. Xiang, R. Wang, J. He, T. Liu, W. Xie, J. Guo, D. Kinghorn, L. Wu, Q. Ji, T. Kippenberg, K. Vahala, J. Bowers, *Nature* **2020**, *582*, 365.
- [37] K. K. Mehta, C. D. Bruzewicz, R. McConnell, R. J. Ram, J. M. Sage, J. Chiaverini, *Nat. Nanotechnol.* **2016**, *11*, 1066.